LABORATORI NAZIONALI DI FRASCATI
SIS – Pubblicazioni

LNF-99/013 (P)
20 Maggio 1999

CONTRIBUTIONS OF THE LNF ARES GROUP TO THE 1999 PARTICLE ACCELERATOR CONFERENCE (PAC99) NEW YORK, MARCH 1999

The ARES Group
M. Castellano[1], L. Catani[2], A. Cianchi[2], M. Ferrario[1], G. Orlandi[2], S. Tazzari[2], F. Tazzioli[1], V. Verzilov[1]

[1)]INFN-Laboratori Nazionali di Frascati Via E. Fermi 40, I-00044 Frascati, Italy
[2)]INFN-Sezione di Roma2, Università di Roma 2 – Tor Vergata, Italy

PACS.: 41.75.Lx; 41.75.Ht; 41.60.m; 7.77.Ka

Presented at the
1999 Particle Accelerator Conference – New York 29 March-2 April 1999

Time Resolved Energy Measurement of the TESLA Test Facility Beam Trough the Analysis of Optical Transition Radiation Angular Distribution

M. Castellano, A. Cianchi, V. Verzilov INFN-LNF CP 13 00044 Frascati (Italy)
L. Catani, G. Orlandi INFN-Roma 2

Abstract

The study of the energy stability along the macropulse of the TESLA Test Facility Linac (TTFL) [1] was obtained by the measurement of the angular distribution of the Optical Transition Radiation (OTR). This technique does not require a dispersive section and can be performed at any point of the beam line.
Measurements have been performed with different settings of the RF low level control and at different values of the beam current. An energy variation along the macropulse was observed in a good agreement with the measured energy spread of the whole macrobunch.
The analysis of the OTR angular distribution pattern allows also, to some extent, to evaluate the beam angular spread.

1 INTRODUCTION

The energy stability along the macropulse of the TESLA Test Facility Linac (TTFL) [1] is the result of an accurate timing between the RF pulse and the beam injection to compensate for the beam loading. A digital feedback and feedforward algorithm takes care of fast and slow fluctuations. A measurement of the energy stability is required for a fine tuning of the algorithm parameters.
Typically, energy and energy spread measurements are performed in the dispersive section at the end of the transport line, where a dipole magnet bends the beam by 20° and drives it to the dump.
Energy variation along the macropulse can be measured by means of the strip-line beam position monitor available in the same dispersive section, but the large beam width, of the same order or larger than the linear range of the monitor, strongly reduces the accuracy of the measure.
Instead, we used the angular properties of the Optical Transition Radiation (OTR) emitted by the beam crossing a thin aluminum foil, to realize a time resolved energy measure. This measure does not require a dispersive section and can be done, in principle, at every section of the accelerator.
A sensor is placed in the focal plane of a thin achromatic lens to allow the imaging of the OTR angular distribution.
The radiation is emitted in a cone of semiaperture $1/\gamma$, γ being the relativistic factor of the incident particles.
In our case the sensor is the cathode of an intensified CCD camera that has several advantages with respect to a normal CCD. It provides the possibility of a fast controlled gate (down to 200 ns), allows a 12 bits dynamics and has a high signal to noise ratio.
We integrated the signal over 1 microsecond. Delaying the gate by steps of 1 microsecond, we could follow the whole macrobunch evolution. To ensure the bunch to bunch stability we repeated the measure several times.

2. RESULTS

We performed two different measures at different stages of the commissioning of TTF.
The first one was realized with the so-called injector I delivering a beam current of 6 mA at a repetition rate of 216 MHz, with a single accelerating module in operation.
A 45° beam splitter was used to perform in the same time the measure of both the beam energy (with the ICCD) and the spot size (with a normal CCD). The reflectivity of the beam splitter depends on the radiation polarization, resulting in a different intensity in the horizontal and vertical planes (see Fig.1.)
We used a thin achromatic lens of f = 200 mm focal length. Peak positions, and hence the beam energy, were found by applying a fit to the profile obtained from the OTR image along the vertical line crossing the center.

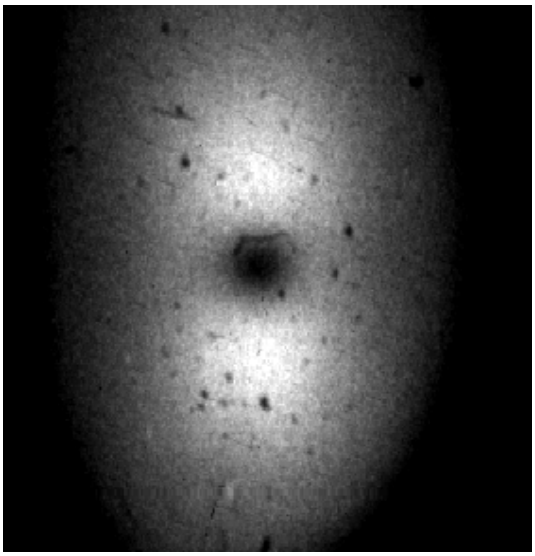

Fig 1 An image of the OTR angular distribution. The difference between horizontal and vertical planes is due to the use of a beam splitter

Fig.2 displays the results of the measurement for two different beam energies.

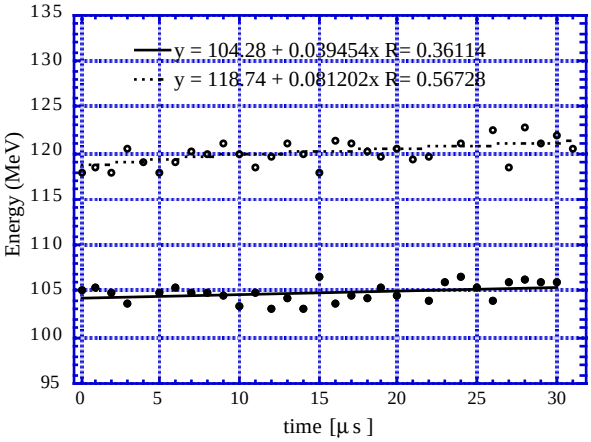

Fig 2 - Variation of the beam energy along the macropulse for two different RF gradients.

In the case of the higher energy, that is the usual working point, the total energy variation along the macropulse is of the order of 2.5%. This result is in a good agreement with the measure made in the dispersive section, which gives a rms energy spread of about 1% over the whole macrobunch.
At a second stage of the commissioning, we operated with the injector II, which supplies a different pulse time structure. The repetition frequency is 1 MHz, so that the integration over 1 microsecond allows the detection of a single micropulse. For these measurements we used a beam current of 1 mA, equivalent to 1 nC of charge for each micropulse, as required for the FEL operation [2].

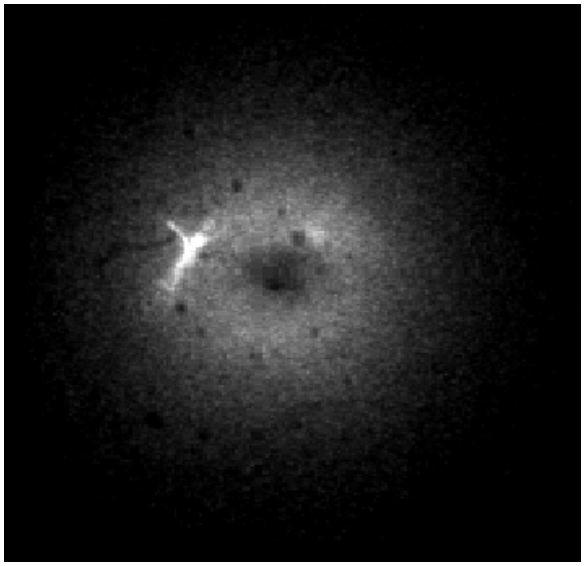

Fig 3 - A typical image of the OTR angular distribution with the injector II

In addition, the installation of a second accelerating module increased the energy of about a factor of 2. In Fig.3 a typical image recorded in this condition is shown.

We performed measurements for three different values of the loop gain in the low-level RF feedback control system for the accelerating modules. This is an important parameter for the control of the gradient during the RF flat top and, thus, of the energy stability along the macropulse. Fig.4 shows the results for the loop gain equal to 44, 36 and 27, respectively.

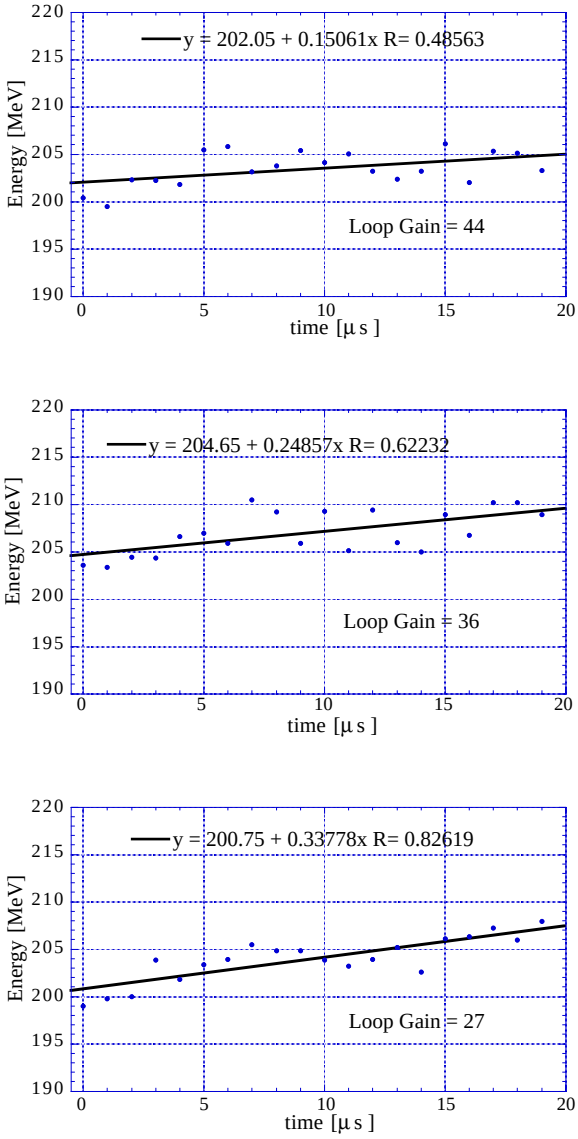

Fig. 4 - Energy variation in the macropulse with three different setting of the RF loop gain

Although the statistical fluctuation of the points is rather large, it is possible to conclude that the energy stability is better at larger values of the loop gain.
A more accurate and systematic work is required in order to determine the best setting for the low-level RF control, and it will be performed in the next run this Summer.

As a by-product of our measurements, we found that an information about the beam angular spread could be obtained by the analysis of the OTR angular distribution profiles.
In Figs. 5 and 6 an example of the vertical profile is presented.

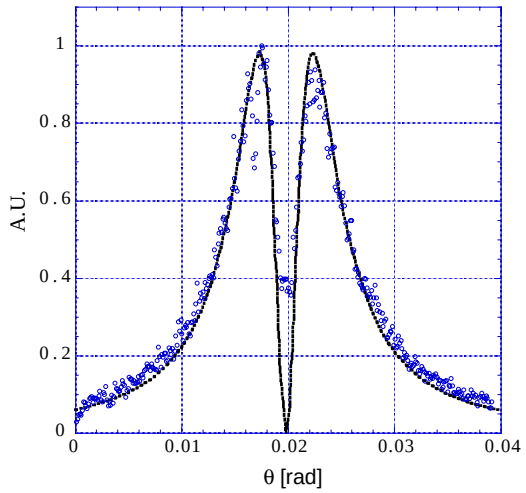

Fig 5 - A profile for the vertical plane of the OTR angular distribution and fitting curve for a parallel beam

The solid line in Fig. 5 is a fit according to the theoretical prediction for a zero divergence beam.
The fit in Fig 6 takes into account the beam divergence and reveals a better agreement with the experimental data.

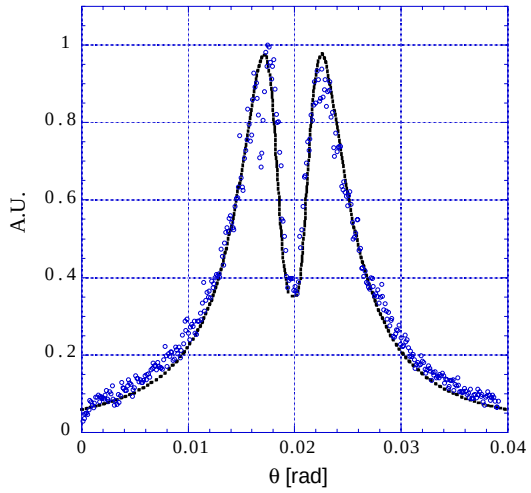

Fig. 6 - Profile of the OTR angular distribution with a fitting function taking into account the beam angular divergence.

A rms angular spread of 0.7 mrad is obtained in this case. Unfortunately, for this data set, in order to avoid the distortion introduced by the beam splitter, we were not able to measure simultaneously the beam spot size. Nevertheless, a spot size value of about 200 μm could be obtained, for the same conditions, from the emittance measurements performed just before. According to this value, a normalized emittance of about 60 mm mrad can be estimated. This is fully consistent with the measured values that ranged from 50 to 100 mm mrad, depending on beam transport conditions.

3. CONCLUSION

We used the properties of the OTR to monitor the energy variation along the macropulse of TTF beam.
Two different measures were performed at different stages of the commissioning, and in both cases we found an increase of the energy along the macropulse.
We have proven that the loop gain value of the low-level RF control can affect the time energy dependence, and that the correct value for this parameter must still be found. A more accurate measurement is needed to explore better this point.
A preliminary analysis shows that it is possible to obtain from the same data also the beam angular divergence, that, together with the measure of the spot size, can give an independent emittance measurement.
To improve the measure accuracy, we plan to use a lens with a longer focal length. A higher number of images for each setting point is also needed in order to reduce the statistical fluctuations.

4 REFERENCES

[1] D. Edwards (editor), TESLA Test Facility Linac – Design Report, DESY TESLA 95-01 (1995)

[2] A VUV Free Electron Laser at the TESLA Test Facility at Desy – Conceptual Design Report
DESY TESLA-FEL 95-03 (1995)

EFFECTS OF DIFFRACTION AND SCREEN SIZE ON CTR BASED BUNCH LENGTH MEASUREMENTS

M. Castellano, A. Cianchi, V. A. Verzilov * INFN-LNF, G. Orlandi INFN-Roma2

Abstract

Coherent transition radiation (CTR) is now well established as one of basic tools to measure electron bunches on a subpicosecond scale. However, a series of experiments has demonstrated that suppression of CTR spectra at low frequencies, occurring in practice, leads to a great uncertainty in the bunch length determination. In addition to known sources of suppression, it was recently found [1, 2] that the size of a screen used to produce transition radiation (TR) can be a factor strongly affecting the spectrum. In this paper we calculate TR spectra emitted by a relativistic electron from a finite-size metallic screen and influenced by diffraction on apertures in environment and collecting optics.

1 INTRODUCTION

Operating with subpicosecond bunches is crucial to the new generation of e^+e^- colliders and FELs for reaching their final goals, which are respectively high luminosity and high peak current. To obtain this result, much depends on the ability to monitor bunch dimensions on such a small scale.

Coherent transition radiation (CTR) is now intensively used for ultra-short bunch length measurements due to its simplicity of implementation and small perturbations produced to the beam.

In this technique the bunch longitudinal dimension can be extracted from the measured CTR spectrum if the incoherent TR spectrum is precisely known [3]. In practice, however, there is a number of experimental factors, such as the limited bandwidth of the detector and diffraction effects due to finite apertures in the radiation transport channel, which cause hardly evaluated losts of the low frequency part of measured spectra, thus leading to a considerable uncertainty in the bunch length and shape determination [4].

Furthermore, the proper role of the size of the target in modifying the power spectrum of incoherent TR was shown [1, 2] recently. It was found that the TR spectrum from a finite target is a complex function of the beam energy, target extensions, frequency and angle of emission, i.e, very different from the flat spectrum given by the Frank formula, that has been used so far. The effect occurs when the parameter $\gamma\lambda$, where γ is the relativistic factor of the beam and λ is the radiation wavelength, exceeds the transverse dimensions of the target.

* Email: verzilov@lnf.infn.it

2 EFFECTS OF DIFFRACTION AND TARGET SIZE ON TR SPECTRA

In the pioneering works [1] the treatment of the problem was performed for a thin layer of matter and TR emitted in the forward direction. As a consequence, the resulting picture of the effect includes interference between TR, the particle field and diffraction radiation and, therefore, is rather complex.

In the present analysis, we rely on the Kirchoff diffraction theory to describe the propagation of the field generated by a charged particle on the boundary between the vacuum and a perfect conducting material [5].TR is considered to emerge in the backward directions with respect to the momentum of the particle crossing the boundary at normal incidence. Three different schemes of measurement, which are simplified models of those typically encountered in practice, are investigated.

2.1 Spectrum of TR filtered by a finite aperture

The first scheme considered is characterized by the presence of a circular diaphragm between the emitting screen and the detector. For ease of calculation we assume a cylindrically symmetric geometry. A circular screen with a radius r made of a perfect metal is placed at a distance a from the diaphragm, while b is the distance between the diaphragm and the detector having a diameter $2d$ (Fig. 1a). The incident particle with charge q and velocity v hits the screen at the center. Emerging TR propagates in the z direction. Let us introduce three different sets of coordinates (x_s,y_s),(ξ,η) and (x,y) for the screen, diaphragm and detector planes, respectively.

In cylindrical coordinates we have:

$$\begin{Bmatrix} x_s \\ y_s \end{Bmatrix} = \rho_s \begin{Bmatrix} \cos\varphi \\ \sin\varphi \end{Bmatrix} , \begin{Bmatrix} x \\ y \end{Bmatrix} = \rho \begin{Bmatrix} \cos\chi \\ \sin\chi \end{Bmatrix} , \qquad (1)$$

Then the TR field components at an arbitrary point P(x,y) in the detector plane in the first order Fresnel approximation of the diffraction theory, and neglecting phase constants, are found to be

$$E_{x,y}(P,\omega) = \frac{q}{2\pi^2 v}\frac{k^2}{ab}\int \mathrm{d}\rho_s \rho_s \int \mathrm{d}k_\perp \frac{k_\perp^2 J_1(k_\perp \rho_s)}{k_\perp^2 + \alpha^2}$$
$$\times \mathrm{e}^{\mathrm{i}(k/2am)\rho_s^2} \int \mathrm{d}\varphi \begin{Bmatrix} \cos\varphi \\ \sin\varphi \end{Bmatrix} \mathrm{e}^{-\mathrm{i}(k/am)\rho\rho_s\cos(\varphi-\chi)} \mathcal{L}(p), \quad (2)$$

where $k_\perp$ is the projection on the xy plane of the the photon wave vector $k = \omega/c$, $\alpha = \omega/v\gamma$, $m = 1 + b/a$, J_1 is the Bessel function of the first kind and

$$\mathcal{L}(p) = 2\pi \mathrm{e}^{\mathrm{i}(k/2bm)p^2} \int_0^D \mathrm{d}\zeta \zeta \mathrm{e}^{\mathrm{i}(km/2b)\zeta^2} J_0(k\zeta p/b), \quad (3)$$

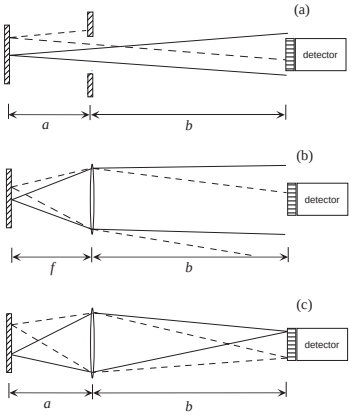

Figure 1: Three schemes of measurements under consideration.

$$p = \sqrt{\rho^2 + (b^2/a^2)\rho_s^2 + 2(b/a)\rho\rho_s \cos(\varphi - \chi)} \; ,$$

As follows from Eq. (2), the field in P is built up by a coherent summation of the waves emitted by all points of the source and so it depends on both the shape and the size of the screen. The function $\mathcal{L}$, mainly determined by the integral over the diaphragm surface, gives a contribution from the standard diffraction by the aperture. The above integral is well known (see, e.g., [6]) and is expressed in terms of the Lommel functions.

Thus, Eq. (2) includes effects given by both the size of the screen and the diffraction produced by the diaphragm. The latter is well known to produce, basically, a low frequency spectrum cutoff, almost entirely defined by the diaphragm aperture and angular acceptance. Hence, from this point on, we found it reasonable to focus our study on that of the screen size. To this end we formally let D tend to ∞.

In terms of the theory of radiation, the phase factor quadratic in ρ_s in Eq. (2) specifies first order corrections to the so-called wave zone (or radiation zone) approximation due to the extension of the source and the sphericity of wave fronts at the point P.

For a finite-size screen these corrections are noticeable if

$$\frac{r^2}{am} \geq \lambda \geq \frac{am}{\gamma^2} \; . \tag{4}$$

and their effect is, in last instance, to reduce the "effective" size of the screen.

It should be noted that these corrections are relevant even for an infinite screen causing it to act like a finite-size one with an "effective" dimension depending on the wavelength and the distance to the observation point, if TR is observed at distances

$$\lambda\gamma^2 \geq z \; . \tag{5}$$

In the far-infrared region, that represents our main interest, the wave-zone condition can be well fulfilled by adjusting the distance between the target and detector, thus allowing to approximate the aforementioned phase factor by 1.

As a consequence of simplifications made, the total spectrum of TR from the finite-size screen, integrated over the detector aperture, in the wave zone is found from Eq. (2) upon a change of variable $\rho = am \sin\theta$:

$$S_\omega = \frac{2q^2}{\pi c}\frac{k^2}{\beta^2}\int_0^{\theta_m} \mathrm{d}\theta \sin\theta\cos\theta\, \Phi^2(r,\alpha,k,k\sin\theta) \; , \tag{6}$$

where $\theta_m = arcsin(d/am)$ is the angular acceptance of the detector and

$$\Phi(r,\alpha,k,\delta) = \frac{\delta}{\alpha^2+\delta^2} - \frac{\alpha r}{\alpha^2+\delta^2}\,[\delta K_1(\alpha r)J_0(\delta r) + \alpha J_1(\delta r)K_0(\alpha r)] - \int_0^r \mathrm{d}\rho_s J_0(k\rho_s)J_1(\delta\rho_s) \; . \tag{7}$$

Here K_n is the modified Bessel function of the n-th order.

Figures 2 and 3 show the spectra calculated by using Eq. (6) for parameters and frequency ranges typical for bunch length measurements, and normalized to the corresponding spectra from an infinite screen.

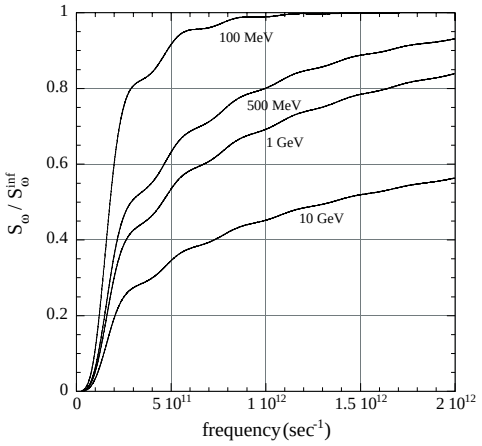

Figure 2: Spectra S_ω of TR in the first scheme of measurements, for a screen with radius of 20 mm and a detector angular acceptance of 0.05 rad.

2.2 *Spectrum of TR from a screen in the focal plane of a lens*

The second scheme under consideration (Fig. 1b) is a simplified geometry normally used in autocorrelation interferometric measurements, when the screen is placed in the front focal plane of a converging lens (parabolic mirror) to produce, behind the lens, a quasi-parallel photon beam.

The analysis performed for a thin lens with diameter $2D$ and focal length f results in the expression for the field identical to Eq. (2) and (4) if one puts $a = f$ and $m = 1$. The power spectrum, in the infinite lens approximation, is, therefore, given by Eq. (6) with

$$\theta_m = arcsin(d/f) \; . \tag{8}$$

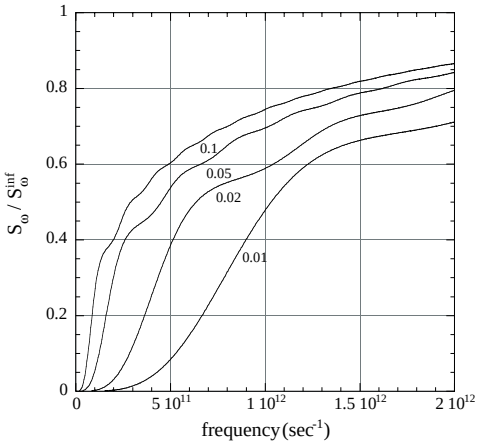

Figure 3: Spectra of TR S_ω in the first scheme of measurements for a screen radius of 20 mm and beam energy of 1 GeV. Numbers next to the curves are detector angular acceptances in radians.

The similarity between the first and second schemes can be seen by simple ray tracing: the effect of the lens is basically to "draw" the detector towards the screen, resulting in an increase of the angular acceptance of the system.

2.3 Spectrum of TR in the screen's image plane

Here the diaphragm of the first scheme is replaced by a lens of the same size and a and b are chosen such that the condition $1/a + 1/b = 1/f$ is satisfied (Fig. 1c). In this geometry the screen is simply imaged onto the detector. The expression for the field is given by

$$E_{x,y}(P,\omega) = \frac{q}{2\pi^2 v}\frac{k^2}{ab}\int \mathrm{d}\rho_s \rho_s \int \mathrm{d}k_\perp \frac{k_\perp^2 J_1(k_\perp \rho_s)}{k_\perp^2 + \alpha^2} \times \mathrm{e}^{\mathrm{i}(k/2a)\rho_s^2}\int \mathrm{d}\varphi \begin{Bmatrix}\cos\varphi \\ \sin\varphi\end{Bmatrix} \mathcal{L}(p)\ , \quad (9)$$

where, as before, $\mathcal{L}$ is the pattern resulting from the diffraction on the lens, that in this case is given by the well-known expression

$$\mathcal{L}(p) = \frac{2\pi a D}{kp} J_1(\frac{kD}{a}p)\ , \quad (10)$$
$$p = \sqrt{\varrho^2 + \rho_s^2 + 2\varrho\rho_s\cos(\varphi - \chi)}\ ,$$

with $\varrho = \rho/M$,where $M = b/a$ is the lens magnification.

For the infinite lens and neglecting the phase factor, the total power spectrum can be given in the form

$$S_\omega = \frac{2q^2}{\pi c}\frac{1}{\beta^2}\int_0^{d/M} \mathrm{d}\varrho\varrho\left[\alpha K_1(\alpha\varrho) - \frac{J_0(k\varrho)}{\varrho}\right]^2\ . \quad (11)$$

In Eq. (11) we imply that $d/M \leq r$, while generally one should integrate from 0 to $\min\{d/M, r\}$.

We want to attract attention to the identical role of the screen and detector dimensions in affecting the spectrum. In fact, since the intensity distribution in the image plane is just a "magnified" image of that in the source plane, both screen and detector are equivalent in producing restrictions on the transverse region over which the power spectrum must be calculated; namely, the spectrum is only determined by the minimum values of d/M and r.

3 EFFECT OF THE SCREEN SIZE IN CTR BASED BUNCH LENGTH MEASUREMENTS

Considering a low-frequency distortion of the TR spectrum due to a finite-size screen in the context of bunch length measurements one can expect that its effect on the accuracy of the bunch information retrieval may be sufficiently small as long as the corrupted portion of the spectrum is negligible compared to the frequency content of the bunch structure represented by the bunch form-factor. For the gaussian-shaped beam the following qualitative criterion can be used to estimate whether for a given bunch length σ_z the effect of the screen size is important

$$\sigma_z < c/\sqrt{2}\omega_{ch}\ . \quad (12)$$

Here ω_{ch} is a characteristic cutting frequency of the spectrum due to the effect. If, as usual for such kind of problems, one defines the cutting frequency as a 10% dropoff of spectra from the high-frequency plateau, simple approximate relations for ω_{ch} may be obtained by analyzing Eqs. (11) and (6), respectively

$$\omega_{ch}(sec^{-1}) = 3.3\cdot 10^9 E^{0.87}(\mathrm{MeV})/\sqrt[4]{\theta_m(\mathrm{rad})} \quad (13)$$

and

$$\omega_{ch}(sec^{-1}) = 8.3\cdot 10^{10} E^{0.87}(\mathrm{MeV})/d(\mathrm{mm})\ . \quad (14)$$

4 REFERENCES

[1] N.F.Shul'ga and S.N.Dobrovol'skii, Pis'ma Zh. Eksp. Teor. Fiz. 65 (1997) 581 [JETP Lett. 65 (1997) 611]. N.F.Shul'ga, S.N.Dobrovol'skii and V.G.Syshchenko, Nucl.Instr. and Meth. in Phys. Res. B 145 (1998) 180 .

[2] A.P.Potylitsin, Nucl. Instr. and Meth. in Phys. Res. B 145 (1998) 169.

[3] W.Barry, AIP Conference Proceedings 390 (1997) 173; Proc. of the 7th Beam Instrumentation Workshop, Argonne, May 1996.

[4] A.Murokh, J.B.Rosenzweig, M.Hogan, H.Suk, G.Travich and U.Happek, Nucl. Instr. and Meth. in Phys. Res. A 410 (1998) 452 .

[5] M.Castellano and V.A Verzilov, Phys. Rev. ST- Accel. Beams 1 (1998) 062801.

[6] M.Born and E.Wolf, *Principles of Optics* (Pergamon Press, New York, 1965).

A SIMPLE DERIVATION OF THE LONG WAVELENGTH EDGE RADIATION FROM A BENDING MAGNETS

M. Castellano#
INFN - Laboratori Nazionali di Frascati - CP 13 - 00044 Frascati - ITALY

Abstract

A simple derivation of the "edge radiation" emitted by an electron beam going through a bending magnet in the directions of its entrance and exit from the magnet itself is presented. This radiation is characterized by wavelengths much longer than the synchrotron radiation critical wavelength in the same magnet.

The far field radiation emitted by an electron following a curved trajectory inside a finite bending magnet can be approximated with any required accuracy by that produced by an electron following a segmented trajectory made of straight lines with sudden change of the velocity direction. The radiation field amplitude produced by a velocity direction change is that of a "prompt" bremsstrahlung in which the velocity module remains constant. The total amplitude is the sum of all the bremsstrahlung amplitudes with their relative phase difference.

For long wavelengths and around the direction of entrance or exit from the magnet, only few terms are required to give a good description of the radiation as compared with exact calculations

1 INTRODUCTION

The so-called "edge radiation" is emitted by an electron beam going through a bending magnet in the directions of its entrance and exit from the magnet itself. It is characterized by wavelengths much longer than the synchrotron radiation critical wavelength in the same magnet. It is considered for possible scientific applications because may be brighter than the analogous radiation emitted along the central trajectory inside the bending magnets.

It has been often assumed that this radiation could depend from the behavior of the magnet fringing field. I will demonstrate that it is only the standard synchrotron radiation from a finite length magnet.

R.A. Bosch has given a simple interpretation [1] that has some validity in the very long wavelength limit and can be considered a "zero order" approximation.

I will give a more general derivation, valid for all wavelengths and emission angles, which coincides with standard synchrotron radiation at short wavelengths.

The starting point is the observation that the far field radiation emitted by an electron following a curved trajectory inside a finite bending magnet can be approximated with any required accuracy by that produced by an electron following a segmented trajectory made of straight lines with sudden change of the velocity direction.

The radiation field amplitude produced by a velocity direction change is that of a "prompt" bremsstrahlung in which the velocity module remains constant. The total amplitude is the sum of all the bremsstrahlung amplitudes with their relative phase difference.

For long wavelengths and around the direction of entrance or exit from the magnet, only few terms are required to give a good description of the radiation as compared with exact calculations [2]. The Bosch approximation consists in considering only the first term.

2 THEORETICAL CONSIDERATIONS

The starting point is the expression of the radiation intensity emitted by a charged particle in an arbitrary accelerated motion [3]

$$\frac{dI^2}{d\omega d\Omega} = \frac{e^2}{4\pi^2 c}\left|\int_{-\infty}^{\infty} \frac{\underline{n}\times\left[\left(\underline{n}-\underline{\beta}\right)\times\dot{\underline{\beta}}\right]}{\left(1-\underline{\beta}\cdot\underline{n}\right)^2} e^{i\omega\left(1-\underline{n}\cdot\frac{\underline{r}(t)}{c}\right)} dt\right|^2$$

in which $\underline{n}$ is the observation direction and $\underline{\beta}$ the particle velocity.

For a particle travelling only once trough a finite length bending magnet, the integral will be performed between the time of its entrance t_o and the time of its exit t_f.

We can always subdivide the integral as a sum of integrals on smaller time intervals

$$\frac{dI^2}{d\omega d\Omega} = \frac{e^2}{4\pi^2 c}\left|\sum_1^f \int_{t_{i-1}}^{t_i} \frac{\underline{n}\times\left[\left(\underline{n}-\underline{\beta}\right)\times\dot{\underline{\beta}}\right]}{\left(1-\underline{\beta}\cdot\underline{n}\right)^2} e^{i\omega\left(1-\underline{n}\cdot\frac{\underline{r}(t)}{c}\right)} dt\right|^2$$

For sufficient short time intervals and long wavelength, we can assume that the phase factor is constant for each integral, so that we can perform an analytical evaluation

$$\frac{dI^2}{d\omega d\Omega} = \frac{e^2}{4\pi^2 c}\left|\sum_1^f e^{i\phi_k}\left[\frac{\underline{n}\times\underline{\beta}}{\left(1-\underline{n}\cdot\underline{\beta}\right)^2}\right]_{k-1}^{k}\right|^2 \qquad (1)$$

#michele.castellano@lnf.infn.it

This corresponds to approximate the curved path of the particle with a segmented trajectory, in which the particle velocity, constant in module, changes suddenly its direction.

The radiation amplitude for each change of direction can be written as that of a particle in uniform motion suddenly stopped, plus that of a particle starting with constant velocity in the new direction. The two amplitudes have opposite sign due to the different accelerations.

This approach of "prompt bremsstrahlung" has proven its efficacy in many radiation processes, from standard transition radiation to undulator transition radiation [4].

For our purpose, we can rearrange the terms of the sum in (1)

$$\frac{dI^2}{d\omega d\Omega} = \frac{e^2}{4\pi^2 c}\left| e^{i(\phi_f-\phi_o)}\left(\frac{\underline{n}\times\underline{\beta}_o}{\left(1-\underline{n}\cdot\underline{\beta}_o\right)^2}-\frac{\underline{n}\times\underline{\beta}_f}{\left(1-\underline{n}\cdot\underline{\beta}_f\right)^2}\right)+\sum_1^f\left(\frac{\underline{n}\times\underline{\beta}_{k-1}}{\left(1-\underline{n}\cdot\underline{\beta}_{k-1}\right)^2}-\frac{\underline{n}\times\underline{\beta}_k}{\left(1-\underline{n}\cdot\underline{\beta}_k\right)^2}e^{i(\phi_k-\phi_{k-1})}\right)\right|^2 \quad (2)$$

The first two terms in (2) represent, respectively, the radiation field amplitude produced by a particle that, moving at constant velocity, stops suddenly at the entrance of the bending magnet, and that of a particle at rest that starts moving in uniform motion at the exit of the magnet. Each of these amplitudes, that are often found in radiation phenomena, as Optical Transition Radiation, produce a radiation angular distribution with a maximum intensity at an angle equal to $1/\gamma$ with respect to the particle velocity, γ being the particle relativistic factor.

If the bending angle caused by the magnet is much larger than $1/\gamma$, the two amplitudes do not interfere, independently of the wavelength, and we have two separate sources each with the properties of a prompt bremsstrahlung. This is the approximation introduced in [1]. In this case the radiation is distributed symmetrically around the direction of entrance and exit of the beam from the magnet, and has a flat spectrum. Exact numerical calculations [2] show that this approximation has some validity only for very long wavelengths, and is not able to give the radiation intensity at larger angles, where the other terms in (2) are much more important.

These terms also are not new in the radiation panorama. Each element of the sum represents the field amplitude produced by a particle starting, from rest, at constant velocity in a given direction and then stopping after a finite path length. In the segmented trajectory model, this represent the radiation amplitude produced by the particle in a single rectilinear segment. This amplitude has been studied in transition radiation emission as the interference between two radiating foils, and, equivalently, but less known, as an under threshold Cherenkov radiation.

To better understand the effects of these terms on the total amplitude, we will analyze the behavior of one of them in the horizontal plane, where its contribution is more sensible.

We have two equal amplitude of opposite sign separated by a phase difference that can be written as

$$\phi = \frac{2\pi d}{\lambda}\left(1-\beta\cos\theta\right)$$

in which d is the distance traveled by the particle and θ is the observation angle with respect to the particle velocity.

The intensity distribution produced by a single segment of the trajectory is given by

$$\frac{dI^2}{d\omega d\Omega} = \frac{e^2}{c}\left(\frac{d}{\lambda}\right)^2 \sin^2\theta\left(\frac{\sin\frac{\phi}{2}}{\frac{\phi}{2}}\right)^2$$

It is clear that the smaller is the ratio d/λ, the lesser is the intensity, but spanning a larger angle range. This must be kept in mind when deciding how segmenting the trajectory and how many terms of the sum in (2) should be considered.

3 NUMERICAL SIMULATIONS

To demonstrate the effectiveness of this approach, I have calculated the radiation angular distribution in the horizontal plane for a real case, i.e. the Super-ACO storage ring, for which exact calculations and measurements exist [2].

The machine parameters relevant for this calculation are summarized in Table 1.

Table 1 – Relevant parameters of Super-ACO

Energy	800	MeV
Bending angle	$\pi/4$	rad
Curvature radius	1.7	m

The large bending angle prevents any interference between amplitudes at the entrance and exit of the magnet, for all reasonable wavelength value, so that the first two amplitudes in (2) can be considered separately.

In the following I will show some example of the radiation angular distribution along the exit direction from the magnet. In this case the first term in (2) can be neglected. In Fig. 1 the effect of a single bremsstrahlung amplitude (second term in (2)) is shown. This corresponds to the "zero length" model presented in [1]. Intensity and angular distribution of the radiation do not depend from wavelength. It must be noted that for practical reasons the intensity is given in arbitrary units, but the scale is the same for all the pictures, which can be directly compared.

Positive angles are towards the inner part of the curved trajectory.

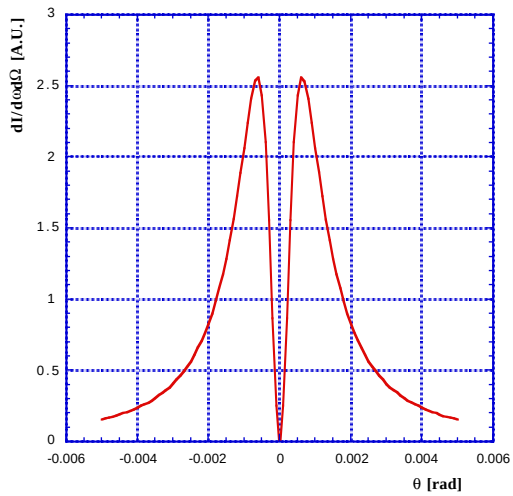

Fig 1 – Edge radiation angular distribution produced by a single bremsstrahlung amplitude

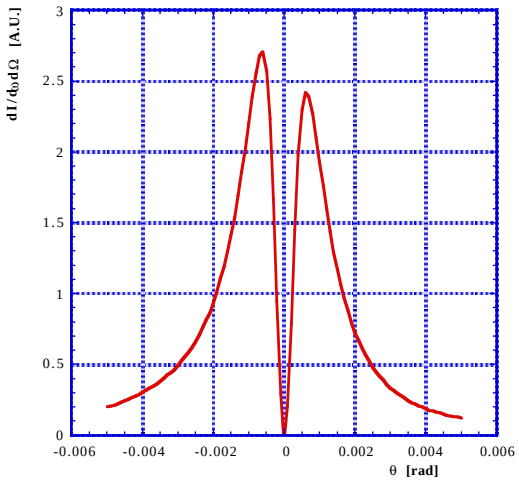

Fig 2 – Angular distribution of edge radiation at 500 μm

In Fig. 2 it is represented the same distribution for a radiation wavelength of 500 μm obtained from (2) approximating the curved trajectory as 15 linear segments, but considering only the contribution of the last three. The asymmetry between the two lobes is now evident, and can be compared with that calculated in [2].

Even if based on a small number of terms, this result is accurate, compared to exact evaluations, to better than 1% on the peaks and to better than 5% on the tails.

Increasing the number of segments and the number of terms considered in (2), the intensity distribution at shorter wavelength can be computed with the same accuracy. As it is shown if Fig. 3, the asymmetry of the lobes increases and the distribution approaches the flat behavior of the "standard" synchrotron radiation.

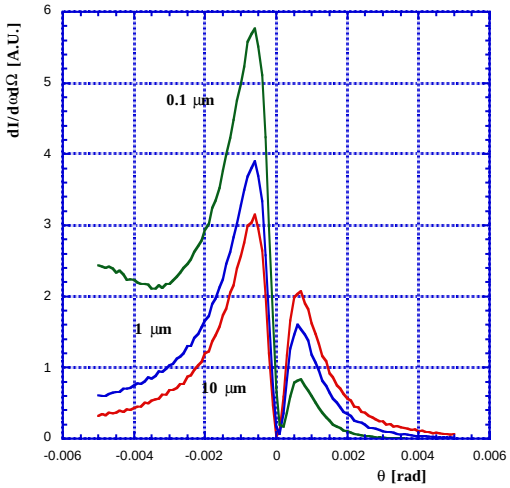

Fig 3 – Edge radiation angular distribution at shorter wavelength

4 CONCLUSIONS

The approximation of the trajectory inside a bending magnet as a sum of straight segments allows an intuitive and simple evaluation of the radiation emitted along the directions of entrance and exit from the magnet. In the case of long wavelengths an accurate result can be obtained by a simple expression. The use of prompt bremsstrahlung amplitudes allows also to consider the interference with other possible source of radiation along the straight section, due to insertion devices or even the mirror used to extract the edge radiation, in a simple way.

5 REFERENCES

[1] R.A. Bosch, Il Nuovo Cimento 20D, 483, (1998)
[2] P. Roy et al., Il Nuovo Cimento 20D, 415, (1998)
[3] J.D. Jackson, Classical Electrodynamics, J. Wiley & sons
[4] M. Castellano, Nucl. Instr. and Meth. in Phys. Res. A391, 375 (1997)

BEAM DYNAMICS SIMULATIONS FOR LINACS DRIVING SHORT-WAVELENGTH FELs

M. Ferrario, F. Tazzioli, LNF-INFN, Frascati
L. Serafini, Univ. of Milan and INFN-Milan

Abstract

The fast code HOMDYN has been recently developed, in the framework of the TTF (TESLA Test Facility) collaboration, in order to study the beam dynamics of linacs delivering high brightness beams as those needed for short wavelength FEL experiments. These linacs are typically driven by radio-frequency photo-injectors, where correlated time dependent space charge effects are of great relevance: these effects cannot be studied by standard beam optics codes (TRACE3D, etc.) and they have been modeled so far by means of multi-particle (PIC or quasi-static) codes requiring heavy cpu time and memory allocations. HOMDYN is able to describe the beam generation at the photo-cathode and the emittance compensation process in the injector even running on a laptop with very modest running times (less than a minute). In this paper we show how this capability of the code is exploited so to model a whole linac up to the point where the space charge dominated regime is of relevance (200 MeV).

1 GENERAL CRITERIA FOR OPTIMIZATION OF A PHOTO-INJECTOR

The art of designing optimized RF Photo-Injectors capable to deliver high brightness electron beams has moved in the last decade from a cut and try procedure, guided by rule of the thumb guesses and going through time consuming simulations, up to a fast parameter space scanning guided by the analytical results of the theoretical model for laminar beams [1], achieved by means of a fast running code based on a multi-beam multi-envelope description of the beam dynamics. By this technique it is possible to study the time dependent space charge problem inherent in the beam dynamics of such devices, so to reach the optimum operating point which corresponds to maximum beam brightness.

The code HOMDYN [2] is actually tailored to describe, within a multi-envelope multi-beam frame, the space charge dominated dynamics of laminar beams in presence of correlated, or time dependent space charge forces: because it's not a multi-particle code, but a multi-envelope one, the code behaves like any beam transport code like TRACE-3D or TRANSPORT, giving rise to very fast modeling capability for photo-injectors.

It has been by now understood that the optimization of a photo-injector corresponds to accelerating and propagating the beam through the device as close as possible to two beam equilibrium, a laminar Brillouin flow (in drifts) and the so-called invariant envelope (in accelerating sections) which is a generalization of Brillouin flow for an accelerated beam. In this case the beam undergoes cold plasma oscillations, i.e. the space charge collective force is largely dominant over the emittance pressure, where the betatron motion (trajectory cross-over) is almost absent (laminar flow) and the frequency of the plasma oscillations due to mismatches between the space charge force and the external focusing gradient is to first order independent on the current. It is such a frequency independence that brings to reversible normalized emittance oscillations: accelerating the beam through the invariant envelope just makes these oscillations damped like the square root of the beam energy, bringing the normalized emittance at the injector exit down to a steady state minimum when the oscillations are properly tuned.

The laminar behavior of an electron beam is characterized by the laminarity parameter

$$\rho \equiv \left\{ \frac{\left[Ig(\zeta)/2I_0 \right]}{\varepsilon_{n,th}\gamma\sqrt{3\gamma'^2/4+\Omega_L^2}} \right\}^2$$

which is defined in terms of the beam average energy γ, the peak current I ($I_0 = 17$ kA), the accelerating gradient $\gamma' = eE_{acc}/mc^2$, the Larmor frequency of the solenoid focusing field $\Omega = \frac{eB_{SOL}}{2m}$ and the rms normalized thermal emittance $\varepsilon_{n,th}$. The beam is said to be laminar whenever $\rho >> 1$, which occurs from the photo-cathode surface up to energies even in excess of 100 MeV for beams carrying about 100 A of peak current.

The time dependence of the space charge field effects is expressed through the geometrical factor $g(\zeta)$, which is a function of the longitudinal position in the electron bunch (the so-called slice position), defined as $\zeta \equiv z - \beta ct + z_0$.

Whenever the geometrical factor $g(\zeta)$ has a significant variation along the bunch, we obtain a beam perveance term in the rms envelope equation, which is slice-dependent, therefore we are in presence of time (or slice) dependent effects. In the case of a cylindrical bunch we have for instance

$$g \cong 1 - \frac{2A^2}{\gamma^2}\left[1 + 12\left(\frac{\zeta}{L}\right)^2 + 80\left(\frac{\zeta}{L}\right)^4\right],$$

showing that when the bunch aspect ratio $A \equiv R/L$ is not much smaller than 1 the dependence on the slice coordinate can be quite relevant.

It has been shown that the rms projected normalized emittance $\varepsilon_n \equiv p\sqrt{\langle x^2\rangle\langle x'^2\rangle - \langle xx'\rangle^2}$ oscillates with a frequency $\sqrt{2K_r}$ at an amplitude $\Delta\varepsilon_n \propto \sqrt{\frac{I\langle g\rangle}{\gamma}}\sqrt{\langle g^2\rangle/\langle g\rangle^2 - 1}$ whenever a bunched beam (i.e. $g(\zeta) \neq 1$) is rms matched into a focusing channel of gradient K_r, i.e. on a Brillouin flow equilibrium $\sigma_B(\zeta) = \sqrt{\frac{Ig(\zeta)}{2I_0\gamma^3 K_r}}$ (where σ is the rms beam spot size, eventually slice dependent). Accelerating on the invariant envelope $\sigma_{inv}(\zeta) = \frac{2}{\gamma'}\sqrt{\frac{Ig(\zeta)}{3I_0\gamma}}$, which is a particular exact solution of the rms envelope equation in the laminar flow regime, brings the emittance to damped oscillations. The basic point in the design of a photoinjector is therefore to match properly the beam at injection into any accelerating section, according to these criteria:

$\hat{\sigma}' = 0$, implying a laminar waist at injection

$\gamma' = \frac{2}{\sigma_w}\sqrt{\frac{I\langle g\rangle}{3I_0\gamma}}$, i.e. an rms match on the inv. env.

These also requires that focusing elements in drifts be spaced close to one quarter of plasma oscillation wavelength, given by $\lambda_p = \frac{4\pi\gamma}{\gamma'}\sqrt{\frac{2}{3}}$.

2 APPLICATION TO THE TTF-FEL LINAC

In this section we study how to implement these matching criteria into the actual design of the TTF linac. up to the end of the second cryomodule, corresponding to a beam energy of 200 MeV. A previous analysis [3] was devoted to a general lay-out for the linac with complete degree of freedom in the spacing of focusing elements and accelerating sections (i.e. the cryostats containing 8 SC accelerating cavities, each with 9 cells working at 1.3 GHz). In the following we will compare those results to the best one can do with the actual lay-out neglecting compressor magnets, not yet implemented in to the code.

The 1 nC beam is generated in one and half cells RF-gun operating at 1.3 GHz with 40 MV/m peak field on the cathode, by a 8 ps (sigma) long laser pulse with 1.5 mm radius. The gun is embedded in a 0.11 T split solenoid field. In the drifting tube downstream the gun the rms emittance reach a first minimum (0.9 mm mrad) corresponding to the minimum ($\sigma'=0$) envelope (σ_r = 1.18 mm) at z=1.2 m from the cathode, where the booster is placed,(Fig. 1).

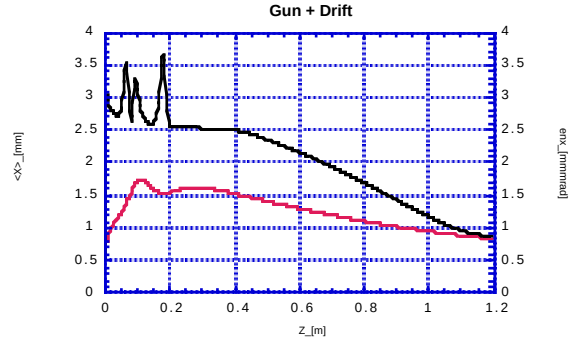

Figure 1: Beam envelope and rms normalized emittance in the gun and drift up to the booster entrance.

To match the booster cavity (9 cells 1.3 GHz superconducting cavity) to the beam we use the previous criteria to compute the accelerating field needed. It results to be 10 MV/m with I=40 A and γ = 10.

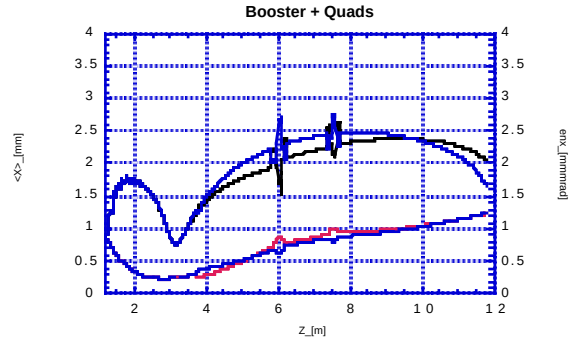

Figure 2: Beam envelope and rms normalized emittance in the booster and drift up to the cryomodule 1 entrance.

Downstream the booster the rms emittance reach a second minimum (0.8 mm mrad) in the drift and at the booster exit (z=2.4 m) the beam envelope (σ_r = 0.35 mm) is still parallel to the z-axis with γ = 35. In the ideal case, as discussed in [3], the envelope should be allowed to perform small oscillations around the equilibrium value reached in the booster and smoothly transported to match the condition $\sigma'=0$ at the entrance of the first cryo-module. The situation is here complicated by the technical constrains of the drift section, foreseen to house focusing elements (one quadrupole doublet and two triplets), diagnostic stations and a chicane compressor. In addition by using quadrupoles as focusing elements the envelope and the emittance oscillations are split in the x and y planes, resulting in a difficult task to match both planes to the cryo-module.

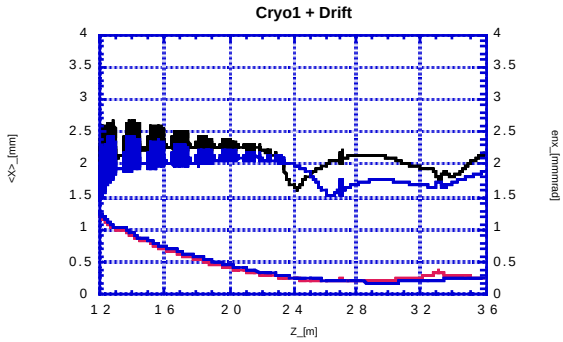

Figure 3: Beam envelope and rms normalized emittance in cryomodule 1 and drift up to the cryomodule 2 entrance.

The best solution we found results to be the less perturbing to the cylindrical symmetry of the beam (Fig. 2). We allowed indeed the envelope to diverge up to σ_r = 1.75 mm with low quadruoles gradients so that to keep the emittance oscillation in phase in both planes up to the entrance of the first cryomodule (z=11.7 m). The beam is there boosted with 11 MV/m accelerating field, a low gradient is chosen to avoid over focussing in the accelerating section. Emittance oscillations are damped during acceleration around 2 mm mrad (Fig. 3).
With the same care the beam is transported to the second cryomodule through a quadrupole focusing channel and boosted up to 200 MeV in the second cryomodule (Fig. 4).

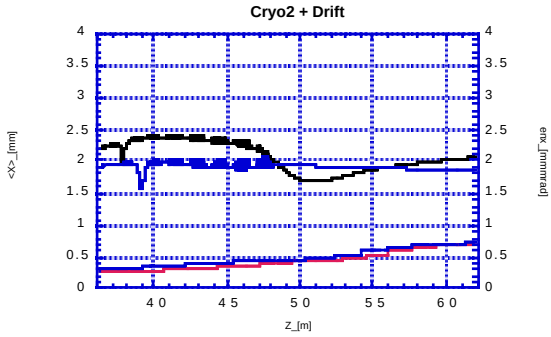

Figure 4: Beam envelope and rms normalized emittance in cryomodule 2 and drift.

4 CONCLUSIONS

By joining the analytical predictions and optimizing criteria produced by the theory of intense relativistic laminar beams with the powerful capability of the new code HOMDYN to model a full photoinjector up to full scale energy (200 MeV) in very short cpu times (minutes on a laptop), the optimization of a new design or the search for the optimum operating point of a present lay-out can be accomplished quickly and easily. We believe that the general design of future injectors will benefit from such a new user-friend procedure.

5 REFERENCES

[1] L. Serafini, J. B. Rosenzweig, "Envelope analysis of intense relativistic quasilaminar beams in rf photoinjectors: a theory of emittance compensation", Phys. Rev. E, **55**, (1997)

[2] M. Ferrario,.A. Mosnier, L. Serafini, F. Tazzioli, J. M. Tessier, "Multi-bunch energy spread induced by beam loading in a standing wave structure", Part. Acc., **52** (1996)

[3] M. Ferrario, L. Serafini, “Multi-bunch dynamics in rf photoinjectors through an envelope equation approach’, Proc. of VI EPAC, Stockholm (1998).

A 90 GHz PHOTOINJECTOR*

D. T. Palmer# and M. J. Hogan, SLAC, Stanford, CA
M. Ferrario and L. Serafini, INFN-Frascati/INFN-Milan, Milan Italy

Abstract

Photocathode rf guns depend on mode locked laser systems to produce an electron beam at a given phase of the rf. In general, the laser pulse is less than σ_z = 10° of rf phase in length and the required stability is on the order of $\Delta\phi$ = 1°. At 90 GHz (W-band), these requirements correspond to σ_z = 333 fsec and $\Delta\phi$ = 33 fsec. Laser system with pulse lengths in the fsec regime are commercially available, the timing stability is a major concern. We propose a multi-cell W-band photoinjector that does not require a mode locked laser system. Thereby eliminating the stability requirements at W-band. The laser pulse is allowed to be many rf periods long. In principle, the photoinjector can now be considered as a thermionic rf gun. Instead of using an alpha magnet to compress the electron bunch, which would have a detrimental effect on the transverse phase space quality due to longitudinal phase space mixing, we propose to use long pulse laser system and a pair of undulators to produce a low emittance, high current, ultra-short electron bunch for beam dynamics experiments in the 90 GHz regime.

1 INTRODUCTION

In this paper we present a detailed rf and beam dynamics design of an 90 Ghz electron source for use as a source of unpolarized electrons for a switched matrix accelerator [1]. RF simulations in both the frequency and time domains were conducted using GdifidL [2]. The beam dynamics simulations were conducted using HOMDYN [3] and ITACA [4]. The design parameters of this injector are listed in Table 1.

2 THEORY

The scaling of a S-band design up to W-band following scaling laws [5] for RF guns brings to on cathode emissivity which are well present state of the art. In fact, since bunch sizes scale like RF wavelength as well as for the bunch charge, that implies that bunch peak current scales invariant while current density scales like the square of the frequency. This leads to a current density in excess of a few MA/cm2 if the BNL/UCLA/SLAC [6] gun design is scaled up to 91 GHz (see Table 1). Furthermore, the cathode RF peak field, as well as the solenoid peak field, scale like the frequency leading to a peak field in excess of 3 GV/m and a solenoid peak field of several Teslas. Because of the tight requirements imposed by a pure scaling, together with the requirement of a laser phase-jitter less than 30 fs, we abandon the conventional scheme for RF guns and adopt a different lay-out.

We follow the scheme presented in [7], where a laser pulse longer than the rf period is sent onto the photo-cathode surface in order to extract a long electron bunch, typically a quarter of the rf wavelength, carrying a modest current, around 20 A. There is no need for phase stability of the laser in this case, not even phase-locking: the accelerating rf field sets up the time structure for the beam. The scaling up to W-band of the lay-out presented in [7] at 1.3 GHz requires a 1.5 GV/m peak field at the cathode and an 11 ps laser pulse generating 170 pC at the cathode surface, of which only 40 will be extracted from the gun. Since the cathode spot size is 120 microns and the extracted current 10 A, the cathode current density is limited to 20 kA/cm2.

Table 1: Nominal S-band operating scaled to W-band for both a pure scaling and the proposed long pulse scaling.

	Nominal S-band Parameters	Scaled W-band Parameters	Scaled W-band Long Laser Pulse
Gradient [GeV/m]	0.140	4.5	1.5
Solenoid Peak Field [T]	0.23	7.3	2.5
Charge [nC]	1	0.032	0.166 (use 1/4)
Laser Pulse Length [ps]	10	0.3	11
Laser-rf Phase Jitter [fs]	1000	30	Anything
Cathode Spot Size [μm]	1000	30	120
Current Density [A/cm^2]	3 x 10^3	>10^6	3 x 10^4

The HOMDYN and ITACA simulations shown in Section 4 show that the linear energy-phase correlation at the front part of the bunch (i.e. the first 30 RF deg), can be transformed into a phase compression using a undulator, achieving a current in excess of 600 A in a sharp peak a few RF degrees long.

3 DESIGN AND MECHANICAL FABRICATION

This rf gun is basically a 1.6 cell BNL/SLAC/UCLA S-Band rf gun scaled to 91.324 GHz. Power is symmetrically feed into the full cell which also has

*Work supported by USDOE DE-AC03-76SF00515
Email: dtp@slac.stanford.edu

symmetrical tuners, as does the half cell. The gun is shown in Figure 1.

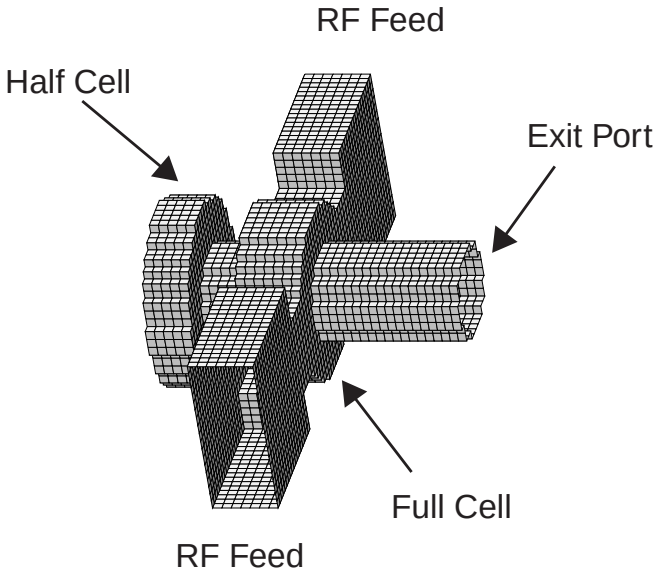

Figure 1: A schematic of the 1.6 cell W-band electron source.

The waveguide to full cell coupling slot is the full height of the full cell. This was decided upon to facilitate the wire EDM manufacturing process The waveguide feed in the body of the gun is not standard WR-10. The waveguide cutoff dimension is still 2.54 mm or 60 GHz. The waveguide height is slightly smaller at 1.016 mm versus 1.27 mm for standard WR-10 waveguide. This decision was determined by our manufacturing technique of wire EDM and our assembly process of high temperature bonding at the high rf current joints. The gun is manufactured out of 5 layers of Glidcop AL-15 [4] to prevent distortion of the cell to cell and rf coupling iris during the thermal cycle necessary for the bonding. The first of these five layers consists of a cathode plate. A half cell plate, which is the thickness of the half cell which is wired EDM. The third plate is the cell to cell iris. The full cell plate which is slightly thinner that the narrow dimension of WR-10 waveguide. It should be noted that the symetric waveguide feed does not extend to the boundary of the material. Only after these five layers are bonded does the waveguide extend to the outer body of the gun. This is to facilitate the alignment and assembly of the gun. The last layer is the exit port of the gun. This layer has the same ID as that of the cell to cell iris. The individually layers of the gun are produced out of a single piece of Glidcop Al-15, in which aligment pin hole are first bored in to the block. A section of this block is sliced off to produce the cathode plate with it alignment pins. A wire start hole is popped through the remaining block. The cell to cell iris is wired into the block and then a section of the block is cut off. This section will be used to manufacture the cell to cell iris and the exit port of the gun. One of the blocks is then sliced into thin section a little thicker than the required cell to cell iris thickness. These will be diamond fly cut flat and parallel to facilitate diffussion bonding. Next the other half of the original block will be cut in half and the full cell cavity and waveguide profile will be wired and sliced as was the case of the half cell. These in turn are also diamond fly cut. The assembly is then cleaned and diffussion bonded. At this point the outer body of the gun is cut to expose the WR-10 waveguide.

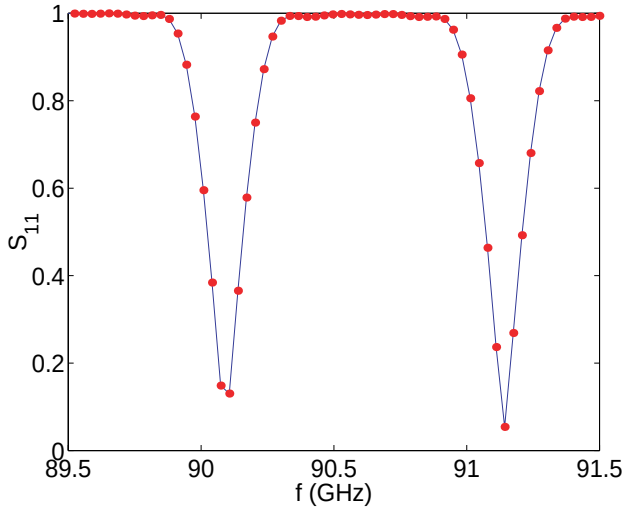

Figure 2: Smith chart reperesnetion of GdifidL smiulations of S_{11}

The rf simulation code GdifidL was ulitized to produce an S_{11} = 1.00 with equal fields at the cathode and in the middle of the full cell (see Figure 2). A Smith Chart representation of this match is shown below in Figurer 3.

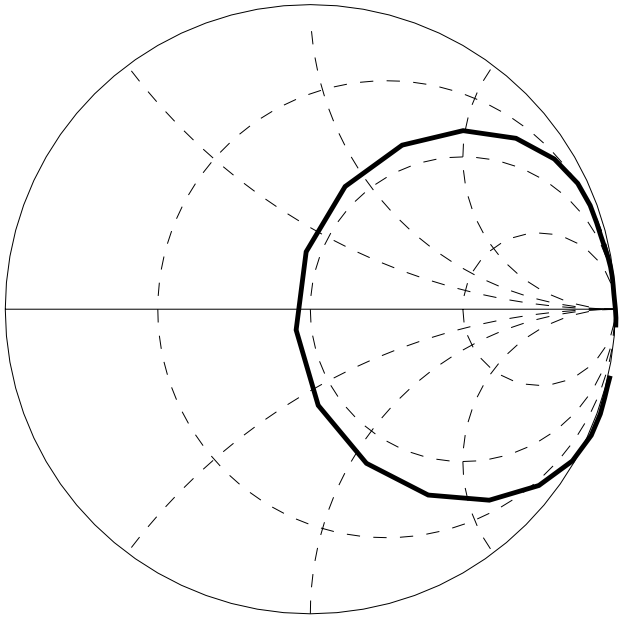

Figure 3: S of both the 0 and pi-modes.

Using the Shunt impedance calculated form Gdifidl we find that the required power from a W-band rf source will in excess of 1 GW.

4 SIMULATIONS

In this section we present a possible configuration for a W-band injector based on a preliminary study of beam dynamics in a system consisting of a 1.5 cell W-band

gun, followed by a solenoid lens, a SW 8 cell booster linac and a short undulator. The gun is 2.5 mm long, the drift up to the booster is 17.5 mm, the booster is 13 mm, the drift up to the undulator is 12 mm and the undulator is 160 mm (8 periods with 2 cm period length).

In order to achieve a nice phase focusing in the gun we have to use a low value for alfa (0.8), resulting in 1.5 GV/m peak field at the cathode. The solenoid lens, located 6.3 mm from the cathode (at z=0), must provide a 2.5 T peak field. The booster linac is run at 500 MV/m accelerating gradient, while the undulator requires a peak field of 0.5 T.

A bunch charge of 166 pC is produced at the photo-cathode surface during the illumination of a 11.1 ps laser pulse (as long as the RF period): because of the low alfa, only the first 65 RF degrees are successfully extracted from the gun, i.e. the first 2 ps of laser pulse lasting from the 0 cathode-field time (0 RF deg) until the 65 RF deg time. The rest of the electrons are either back-accelerated onto the cathode after leaving the cathode surface (those between 65 and 180 RF deg) or not even extracted because of the wrong sign in the applied field (those between 180 and 360). The nominal current in the extracted electron bunch is 15 A (30 pC in 2 ps), implying a cathode current

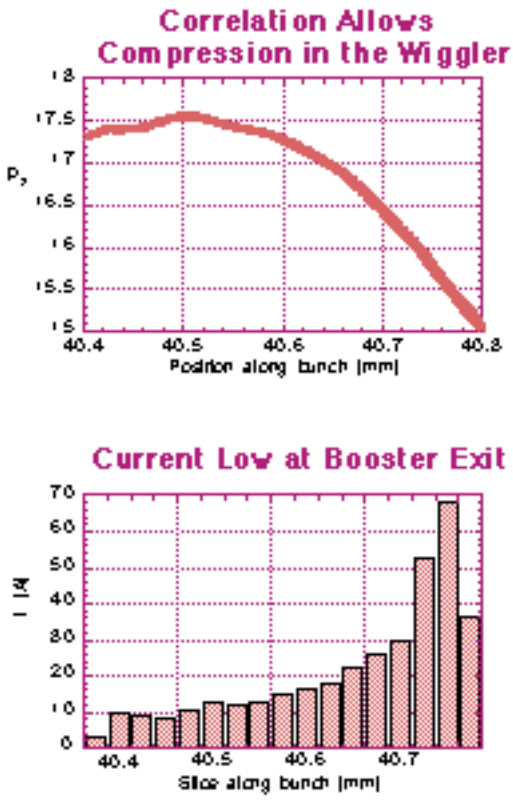

Figure 4: Correlated head of bunch at booster exit.

density of 33 kA/cm^2 at a cathode spot size of 120 microns (as was used in the simulations). The bunch is then focused by the solenoid lens, which is needed to overcome the RF defocusing kick, and injected almost collimated into the booster, which brings up its energy to 7.8 MeV (at the gun exit 1.8 MeV). As a result of the huge phase spread, the energy spread is but nicely linearly correlated in the head part of the bunch (the first 20 RF degrees from z=40.65 to z=40.8, the bunch has just exited the booster). The effect of phase-focusing, achieved thanks to the operation at low alfa, brings a density compression in the head part of the bunch, as shown in Figure 4, plotting the local current carried by the bunch, which is much larger than the nominal value in the head part while much lower in the tail: because of the phase-focusing one obtains peak currents around 70 A, a factor 4 larger than the nominal value.

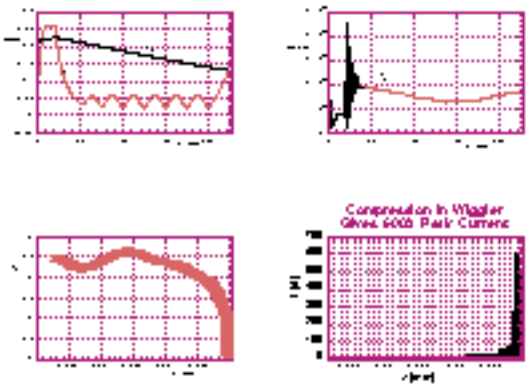

Figure 5: ITACA output of Gun, booster and undulator showing: the bean envelopes, emittance, longitudinal phase space, and peak current.

The beam is further injected into an undulator (no other focusing lenses were used in the short drift to the undulator) that acts like a dispersive medium boosting the phase compression mechanism which would take place anyway even in a simple drift, because of the negative correlation in the energy-phase correlation of the bunch (head particles less energetic than tail particles).

5 REFERENCES

[1] David H. Whittum and Sami G. Tantawi, SLAC-PUB-7848.

[2] Gdifidl

[3] HOMDYN, M. Ferrario, private communication.

[4] ITACA, L. Serafini, private communication.

[5] J. Rosenzweig, E. Colby, AIP 335 (1995) 724

[6] D. T. Palmer, The Next Generation Photoinjector, Ph.D. Thesis, Stanford University.

[7] N. Piovella et al., Proc. of EPAC98, Ed. S. Myers, IoP Publ., Bristol, 1998, p.1465.

EFFICIENT PHOTOEMISSION FROM ROBUST FERROELECTRIC CERAMICS

I. Boscolo, University and INFN, Via Celoria 16, 20133 Milano, Italy
M. Castellano, L. Catani, M. Ferrario, F. Tazzioli, INFN-LNF,
Via E. Fermi, 00044 Frascati - Roma, Italy
L. Giannessi, ENEA-CRE, Via E. Fermi, 00044 Frascati - Roma, Italy

Abstract

Experimental results on photoemission by ferroelectric ceramic disks, with a possible interpretation, are presented. Two types of lead zirconate titanate lanthanum doped, PLZT, ceramics have been used for tests. 25 ps light pulses of 532 and 355 nm were used for excitation. The intensity ranged within the interval 0.1-3 GW/cm^2. The upper limit of the intensity was established by the damage threshold tested by the onset of ion emission. At low value of the intensity the yield was comparable at the two wavelengths. At the highest intensity of green light the emitted charge was 1 nC per 10 mm^2, but it was limited by the space charge effect. In fact, the applied field was only 20 kV/cm, allowed both by the mechanical design of the apparatus and the poor vacuum, 10^{-4} mbar. No surface processing was required. The measurement of the electron pulse length under way.

1 INTRODUCTION

Lead zirconate titanate lanthanum doped (referred as PLZT) ferroelectric ceramic showed interesting properties as photoemitter material [1, 2]: this type of photo-cathode showed an emissivity higher than that of metals, they were able to emit at any photon energy from green to UV and they were very robust, they did not need any processing and, furthermore, they did not require high vacuum condition.

An experimental program has been set at the LNF (Lab Nationali Frascati-Roma) based on the fact that the properties of this material can be determined simply changing the compositional percentage and changing the polarization state. The physical state of the surface is strongly changed by prepoling and by setting a polarization state. In particular, it seems possible to set a polarization state such that the surface electrons are acted on by a repulsive force, or, alternatively, it is possible to set at the surface a very dense sheet of electrons[3].

The sketch of the experimental setup is shown in fig.1. Two incidence angles were used: 60^o and 0^o. In the latter case a hollow Faraday cup with a front grid was used. No variation of the yield was measured for the two configurations.

The experimental program started with the material good for emission with electric excitation [4, 5], that is PLZT 8/65/35 and 4/95/5, where the numbers refer to lanthanum (in relation to lead), zirconium and titanium relative atom percentage. Samples without and with prepoling, at room temperature, were tested. Ceramic 8/65/35 is in ferroelectric phase, while 4/95/5 is in antiferroelectric phase. These materials have a high density of defects whose activation energy is about 1 eV [6]. The cathodes are disks of 16 mm diameter and 1 mm thickness, coated by a uniform metallic film at the back surface and by either an external ring or a grating at the front surface, see fig.1 b). The best results came with the ring front electrode and 8/65/35 unprepoled samples.

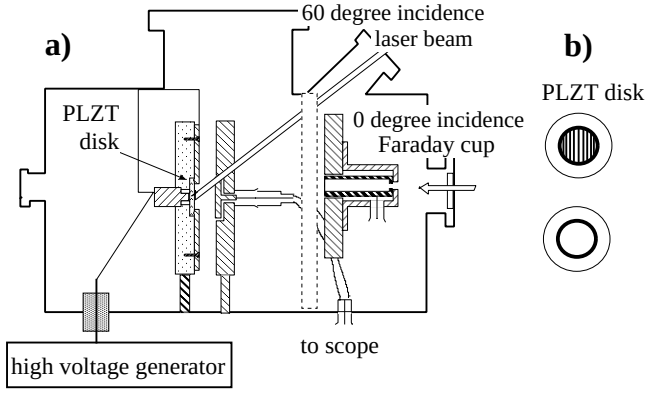

Figure 1: a) Sketch of the experimental apparatus used in the photoemission experiments: the two used Faraday cups are shown for simplicity on the same figure (one behind the other); they are interchanged depending on the incidence angle. b) Sketch of the cathode with the two front electrodes used in tests. The passively mode locked Nd-YAG laser provides some mJ of light at λ = 532 nm for a pulse length of 25 ps. The illuminated area was about 10 mm^2

2 EXPERIMENTAL RESULTS

The emission in the log-log diagram from a PLZT 8/65/35 is shown in figs. 2 and 3. The emission was limited by the space charge effect in the case of green light shining, it was not in the case of violet light shining.

The damage threshold has been checked reversing the direction of the accelerating field. In fig. 4 it is shown that the energy at which the ion emission starts is farther than the beginning of the space charge effect.

From figs. 2 and 3 we notice: a threshold with green light, a yield of an angular coefficient nearby 4 for green light and nearby 3 for violet light. Extrapolating with an

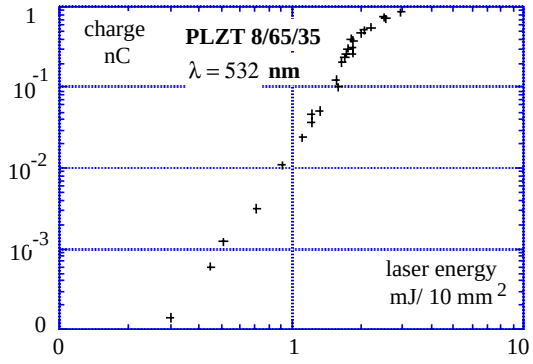

Figure 2: Emitted charge versus laser energy for PLZT 8/65/35 shined with green light in log-log frame. The line fitting the points scales as $Q\alpha I^4$.

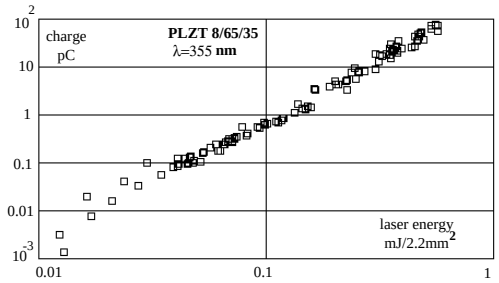

Figure 3: Emitted charge versus laser energy for PLZT 8/65/35 shined with violet light in log-log frame. The slope of the line is $Q\alpha I^3$.

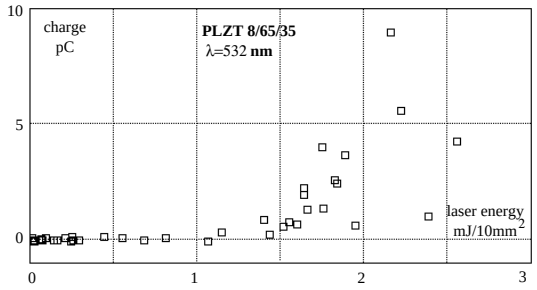

Figure 4: Starting of emission of ions versus laser energy with green light.

accelerating field high enough to avoid saturation effects, the emitted charge at 3 mJ of laser light would be 2 nC. The value of quantum efficiency results around 10^{-6} with both wavelengths.

With violet light we could shine with an energy up to 0.5 mJ only.

The experiments with the antiferroelectric material 4/95/5 and hard ferroelectric material *lead titanate* (PT) gave a much lower yield. The 4/95/5 material showed quite a high enhancement of the yield increasing the accelerating field in the gap as shown in fig. 5. It is notable that this antiferroelectric material shows an hysteretic behavior as function of the applied voltage.

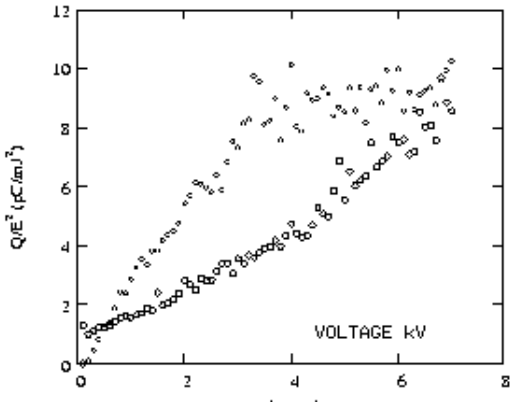

Figure 5: Emitted charge versus laser energy: the lower points are obtained at 7 kV of applied voltage, while the points of the upper curve are obtained in succession but after having reduced the voltage to 3.5 kV. The hysteretic behavior was not observed keeping constant the voltage.

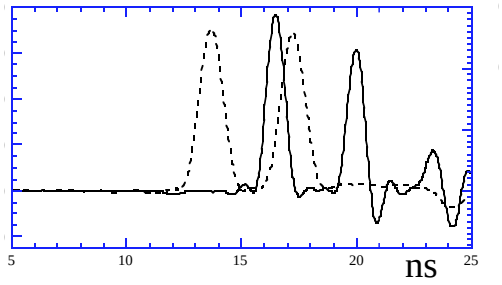

Figure 6: Succession of two electron pulses 2 ns apart

All the tested ceramics had the scaling law $Q\alpha I^2$ at relatively low light flux for both wavelength.

We have tested the emission with two light pulses separated by 2 ns 6. The two emissions are substantially stable. The system seems able to provide pulse trains with nanosecond time separation.

The yield of the prepoled samples was higher than that of the unprepoled ones, but the damage threshold was considerably lower. They showed an emission law which was a bit faster than the two photon emission, but the relatively low damage threshold did not allow an efficient emission.

3 DISCUSSION

The two main characteristics of the strong emission are: a very low emission up to a laser intensity of about 0.5 GW/cm^2 and the high non-linearity starting from that point. In addition to this, the other notable fact is the change of the operational regime for the PLZT 4/95/5 sample when it is immersed in a relatively high electric field.

The energy diagram of the material shows a trap level at 1 eV from the conduction band and has an estimated electron affinity of 3 eV. The electron affinity E_a is not well defined because the surface state is un-defined: is like a

patchwork of pieces with different physical characteristics, which range from insulating to metallic [8]. A value of the potential barrier greater than 4 eV is a fairly crude approximation. The quadratic power law of the emission at both photon energy of 2.3 and 3.4 eV is congruent with the energy diagram.

Furthermore, our disk is immersed in the electric field applied through the diode gap, hence a counter field is created by the induced polarization. When the crystal is polarized, there is a band bending at the surfaces with a potential well for electrons at the positive side of the polarization.

The generalized Fowler-Dubrige theory [7] cannot explain these results. The emission at 2.3 eV and its nonlinearity with a power equal or greater than 4 would envision the anomalous heating regime [9], cooperating with the Auger effect [3]. More generally, we should have the concurrence of different contributions: one and two-photon emission, thermally assisted and Auger emission.

The increase of the emission of 4/95/5 sample as a function of the applied field, together with its hysteretic behavior of fig. 5 tells that the polarization is very important: when the polarization builds up in the sample, the emission steps up, then the sample remains polarized when the electric field is reduced because of the hysteresis loop. The experiment with PT material says that the polarization by itself is not sufficient for obtaining strong emission, but a strong doping, that is a large number of defects, must be also present.

Assuming that the electron pulse length is strictly correlated to the light pulse length, that is $\approx 25ps$, since the illuminated area is about 10 mm^2, the current density would be higher than 1 kA/cm^2.

4 CONCLUSIONS.

A new very efficient configuration for ferroelectric photocathodes has been investigated. We got 1nC level of emission only because the charge was limited by space charge effect. Since the damage threshold of a ceramic is relatively high, a large amount of extracted charge can be foreseen.

The emission has shown to be very sensitive to the sample polarization. This fact allows to foresee a large enhancement of the quantum efficiency just increasing the polarization. This polarization increasing occurs naturally with the high electric field that are applied in electron guns.

The characteristics of these cathodes, are: a)strong robustness, they work in any kind of vacuum showing a long life; b) they do not require any particular processing; c)they can be operated with green light. In the next future the extracted electron beam will be characterized in terms of time structure. If the electron pulse duration is strictly related to the laser pulse duration, these cathodes promise to deliver current densities larger than 1 KA/cm^2 and to be valid competitors of both metallic and alkali cathodes.

5 ACKNOWLEDGEMENTS

We recognize the technical support given by R. Sorchetti and L. Cacciotti.

6 REFERENCES

[1] K. Geissler, H. Gundel, H. Riege, J. Handerek, Appl. Phys. Lett. 56, 895, 1990.

[2] K. Geissler, A. Meineke, H., Riege, S. DE Silvestri, N. Nisoli, O. Svelto, I. Boscolo, J. Handerek, Nucl. Instrum. Meth. Phys. Res.A 372, 567-571,1996

[3] G. Benedek, I. Boscolo, Appl. Phys. Lett. 72, 522, 1998.

[4] G. Benedek, I. Boscolo, J. Handerek, A. Moscatelli, A. Scurati, J. Appl. Phys, 83,2776,1998.

[5] I. Boscolo et al. Appl. Phys. Lett. 74,859,1999.

[6] H. Gundel, J. Handerek, H. Riege, E.J.N. Wilson and K. Zioutas, Ferroelectrics 109,137,1990.

[7] J.H. Bechtel, W.L. Smith, N. Bloembergen, Phys. Rev. B. 15, 4557, 1977.

[8] K. Szot, W. Speier, J. Herion, Ch. Freiburg, Appl. Phys. A 64,55,1997.

[9] J. P. Girardeau-Montaut, C. Girardeau-Montaut, Phys. Rev. 51, 13560, 1995.